Transfer-Matrix Approach to Classical Systems

T. Nishino[1], K. Okunishi[2], Y. Hieida[2], T. Hikihara[1], and H. Takasaki[1]

[1] Department of Physics, Graduate School of Science and Technology, Kobe University, Inoshishi-dai, Nada, Kobe 657-8501, Japan
[2] Department of Physics, Graduate School of Science, Osaka University, Toyonaka, Osaka 560-0043, Japan

The establishment of the DMRG by White [1] is one of the major achievements in computational condensed matter physics (Chap. 2(I)). DMRG enables one to calculate ground states of relatively large scale one-dimensional (1D) quantum systems. Since 1D quantum systems are deeply related to 2D classical systems, [2–4] it is natural to import DMRG method to 2D classical systems. The infinite system algorithm was first applied to the Ising model by one of the authors. [5] Carlon *et al* [6–8] applied the finite system algorithm to the Potts model (Chap. 3.2(II)), and they calculated very accurate density profiles and critical indices. After that, the DMRG formulation for classical systems was applied to 1D quantum system at finite temperature (Chaps. 6(I) and 4(II)). [9,10,12]

In this review we explain the DMRG applied to 2D classical systems (classical DMRG) by looking at the renormalization group (RG) transformation for the transfer matrix T. We therefore first introduce the infinite system algorithm. (§1 - §4) For the distinction, we call the DMRG for quantum systems as 'quantum DMRG' in the following. It is then naturally drawn that classical DMRG is a kind of variatonal method, that maximizes the partition function using a limited degree of freedom, where the variational state is written in a product of local matrices. [15] (§5) Actually, such a variational formulation have been used for long time; we give a brief review in §6. The variational state obtained by the infinite system algorithm can be improved systematically by use of the finite system algorithm. (§7) As a variation of the infinite system algorithm, we introduce the corner transfer matrix (CTM) formulation of the classical DMRG, where the formulation can be generalized to higher dimensional systems. (§8) We finally discuss the remaining problems in the last section.

1 Transfer Matrix

As an example of 2D classical systems, let us consider the square lattice Ising model [17] on a cylinder, which is defined by imposing the periodic boundary condition in the vertical direction of N (= horizontal width) by ℓ (= vertical length) spin lattice; we consider the open boundary condition

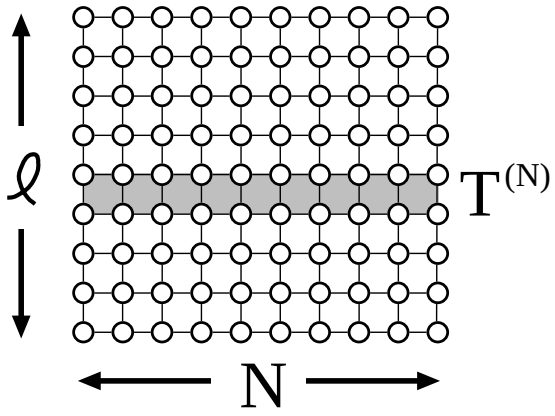

Fig. 1. We consider a square lattice Ising model on an N by ℓ rectangular, which is constructed by stacking ℓ numbers of transfer matrices $T^{(N)}$ defined in Eq.1. We impose the open boundary condition to the horizontal direction, [16] and periodic boundary condition to the vertical direction.

for the horizontal direction. [16] (Fig.1) The system consists of ℓ numbers of rows of width N. We assume $\ell \gg N$, and refer N as the system size. We label the spins in a row from the left to right as $s_1, s_2, \cdots, s_{N-1}, s_N$, where we occasionally write them using the vector notation $\boldsymbol{s} = s_{1\cdots}s_N$ for book keeping. When the Ising interaction is restricted to the nearest neighbor pairs, the transfer matrix is expressed as a 2^N-dimensional matrix (Fig.2)

$$\begin{aligned} T^{(N)}(\boldsymbol{s}'|\boldsymbol{s}) &= \exp\left\{\frac{K}{2}\sum_{i=1}^{N-1}(s'_i s'_{i+1} + s_i s_{i+1}) + K\sum_{i=1}^{N} s'_i s_i\right\} \\ &= \exp\left(\frac{K}{2}s_1 s'_1\right)\left\{\prod_{i=1}^{N-1} W(s'_i s'_{i+1}|s_i s_{i+1})\right\}\exp\left(\frac{K}{2}s_N s'_N\right), \end{aligned} \tag{1}$$

where $K = J/k_{\rm B}T$, and where

$$W(s'_i s'_{i+1}|s_i s_{i+1}) = \exp\left\{\frac{K}{2}\left(s_i s_{i+1} + s_{i+1}s'_{i+1} + s'_{i+1}s'_i + s'_i s_i\right)\right\} \tag{2}$$

is the local Boltzmann weight for a square between i and $i+1$. We have symmetrized the transfer matrix in order to simplify the following formulation. It may be helpful for the readers to remind the quantum-classical correspondence $T^{(N)} = \exp(-\Delta H^{(N)})$, where $H^{(N)}$ is the corresponding quantum Hamiltonian. (Normally $H^{(N)}$ is non-local, unless the model is solvable. The correspondence is therefore rather formal than realistic.)

For a tutorial purpose, we only consider the symmetric transfer matrix in the following. Extensions to the asymmetric case is straight forward; [5,18] to treat an asymmetric transfer matrix is not rare in the classical statistical mechanics. The detail will be explained by Xiang and Wang in Chaps. 6(I), 4.1(II) [10,11] as well as by Shibata in Chap. 4.2(II). [12,13] More generally, it is possible to treat various models such as

- The q-state Potts model [19,20] or the n-vector model, that have *discrete spin symmetry and short range interaction.*
- The interaction round a face (IRF) model [18] whose Boltzmann weight $W(s_i' s_{i+1}' | s_i s_{i+1})$ is represented by arbitrary matrix; *even the weight can be negative.* [14] (There is no sign problem.)
- The vertex model [18] that has spin variables in the middle of each bond.

in the framework of DMRG.

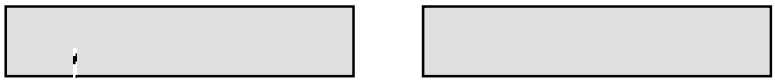

$$T_R(\boldsymbol{s}'_R|\boldsymbol{s}_R) \;=\; \exp\left(\frac{K}{2}s'_N s_N\right) \prod_{i=M+1}^{N-1} W(s'_i s'_{i+1}|s_i s_{i+1})\,. \tag{4}$$

2 Density Submatrix

The density matrix of the N by ℓ system (Fig.1) is simply the ℓ-th power of the transfer matrix $\rho = (T^{(N)})^\ell$. The partition function is its trace

$$Z \;=\; \mathrm{Tr}\,\rho \;=\; \mathrm{Tr}\,(T^{(N)})^\ell \;=\; \sum_\kappa {\lambda_\kappa}^\ell\,, \tag{5}$$

where λ_κ is the eigenvalue of $T^{(N)}$ in the decreasing order $\lambda_1 \geq \lambda_2 \geq \cdots \geq 0$. (We have assumed that the transfer matrix is diagonalizable, and that all the eigenvalues are positive.) Since we have assumed that ℓ is sufficiently larger than N, the partition function can be approximated as $Z \;\simeq\; {\lambda_1}^\ell$, where the symbol '$\simeq$' denotes that the ratio ${\lambda_1}^\ell/Z$ converges to unity in the limit $\ell/N \to \infty$. Under this situation, the density matrix can be well approximated as

$$\rho \;\simeq\; |v^{(N)}\rangle\, {\lambda_1}^\ell\, \langle v^{(N)}| \tag{6}$$

where $|v^{(N)}\rangle$ is the eigenvector of $T^{(N)}$ that corresponds to the largest eigenvalue λ_1. We assume the normalization $\langle v^{(N)}|v^{(N)}\rangle = 1$.

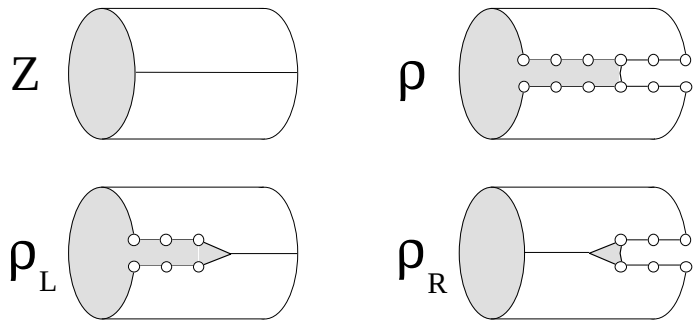

Fig. 3. Graphical representation for ρ, Z (Eq.5), ρ_L and ρ_R (Eq.7). The DSM can be interpreted as a cut on the 2D system shown in Fig.1.

What is called 'density matrix' in the context of DMRG is not the density matrix itself, but is the density submatrix (DSM) — also called as 'reduced

density matrix' — which is obtained by partially tracing out spin indices from ρ. The DSM for the left and the right halves of the system are defined as [21]

$$\begin{aligned}\rho_L(\boldsymbol{s}'_L|\boldsymbol{s}_L) &= \sum_{\boldsymbol{s}_R} \rho(\boldsymbol{s}'_L\,\boldsymbol{s}_R|\boldsymbol{s}_L\,\boldsymbol{s}_R)\\ \rho_R(\boldsymbol{s}'_R|\boldsymbol{s}_R) &= \sum_{\boldsymbol{s}_L} \rho(\boldsymbol{s}_L\,\boldsymbol{s}'_R|\boldsymbol{s}_L\,\boldsymbol{s}_R)\,.\end{aligned} \tag{7}$$

Figure 3 shows the graphical representation of the DSM, where ρ_L and ρ_R correspond to the cuts on the cylindrical system shown in Fig.1. [22] To take the trace of DSM is to join the cut and to reconstruct the cylinder: $Z = \mathrm{Tr}\,\rho_L = \mathrm{Tr}\,\rho_R$. Using the eigenvector $v^{(N)}$ in Eq.6, we can express the DSM in the more familiar form

$$\begin{aligned}\rho_L(\boldsymbol{s}'_L|\boldsymbol{s}_L) &\simeq \sum_{\boldsymbol{s}_R} v^{(N)}(\boldsymbol{s}'_L\,\boldsymbol{s}_R)\,{\lambda_1}^{\ell}\,v^{(N)}(\boldsymbol{s}_L\,\boldsymbol{s}_R)\\ \rho_R(\boldsymbol{s}'_R|\boldsymbol{s}_R) &\simeq \sum_{\boldsymbol{s}_L} v^{(N)}(\boldsymbol{s}_L\,\boldsymbol{s}'_R)\,{\lambda_1}^{\ell}\,v^{(N)}(\boldsymbol{s}_L\,\boldsymbol{s}_R)\end{aligned} \tag{8}$$

that have been used for the quantum DMRG.

As for the quantum DMRG, the diagonalization of the DSM is one of the important step for the classical DMRG. The DSM ρ_L and ρ_R can be diagonalized as

$$\rho_L = \sum_{\xi} \boldsymbol{a}_\xi\,{\omega_\xi}^2\,{\boldsymbol{a}_\xi}^T\,, \qquad\qquad \rho_R = \sum_{\zeta} \boldsymbol{b}_\zeta\,{\mu_\zeta}^2\,{\boldsymbol{b}_\zeta}^T\,, \tag{9}$$

where $\boldsymbol{a}_\xi$ and $\boldsymbol{b}_\xi$ are the eigenvectors of ρ_L and ρ_R, respectively. The eigenvectors satisfy the orthogonal relations ${\boldsymbol{a}_\xi}^T\boldsymbol{a}_{\xi'} = \delta_{\xi\xi'}$ and ${\boldsymbol{b}_\zeta}^T\boldsymbol{b}_{\zeta'} = \delta_{\zeta\zeta'}$, and they are complete

$$I_L = \sum_{\xi} \boldsymbol{a}_\xi\,{\boldsymbol{a}_\xi}^T\,, \qquad\qquad I_R = \sum_{\zeta} \boldsymbol{b}_\zeta\,{\boldsymbol{b}_\zeta}^T\,, \tag{10}$$

where I_L and I_R are 2^M- and 2^{N-M}-dimensional unit matrices, respectively; $I_L = I_R$ when $N = 2M$. It is convenient to use the matrix notation $A = (\boldsymbol{a}_1, \boldsymbol{a}_2, \cdots)$ and $B = (\boldsymbol{b}_1, \boldsymbol{b}_2, \cdots)$ when we explicitly show the spin indices. For example, Eq.9 can be written as

$$\begin{aligned}\rho_L(\boldsymbol{s}'_L|\boldsymbol{s}_L) &= \sum_{\xi} A(\boldsymbol{s}'_L|\xi)\,{\omega_\xi}^2\,A(\boldsymbol{s}_L|\xi)\\ \rho_R(\boldsymbol{s}'_R|\boldsymbol{s}_R) &= \sum_{\zeta} B(\boldsymbol{s}'_R|\zeta)\,{\mu_\zeta}^2\,B(\boldsymbol{s}_R|\zeta)\,.\end{aligned} \tag{11}$$

In Eqs.9 and 11 we have expressed the eigenvalues of ρ_L and ρ_R as squares of real numbers, because normally they are non-negative. [23] As the eigenvalues of ρ, we assume the decreasing order for both ${\omega_\xi}^2$ and ${\mu_\zeta}^2$

$$ {\omega_1}^2 \geq {\omega_2}^2 \geq \cdots \geq 0\,, \qquad\qquad {\mu_1}^2 \geq {\mu_2}^2 \geq \cdots \geq 0\,, \tag{12} $$

in the following. In general, $\omega_i = \mu_i$ holds for $1 \leq i \leq \min(2^M, 2^{N-M})$ in the limit $\ell/N \to \infty$.

3 Renromalization Group Transformation

Unlike the density matrix ρ, not only the largest eigenvalue is dominant in Eq.12. This is because $\boldsymbol{s}'_L$ and $\boldsymbol{s}_L$ in $\rho_L(\boldsymbol{s}'_L|\boldsymbol{s}_L)$ are correlated to through the junction $\boldsymbol{s}_R$. (Eqs.7-8) It has been known that the eigenvalue ${\omega_i}^2$ (or ${\mu_i}^2$) in Eq.12 decays nearly exponential when the correlation length of the system is finite (Chap. 3.1(II)), [18,24,25] and that the decay is rapid when the correlation length is short. Even at the critical temperature, we expect a certain decay in ${\omega_i}^2$, because the system size N is finite and the correlation length is of the order of N. As a result we can say that the partition function can be approximated by the partial sum of the DSM eigenvalues

$$ \tilde{Z} \;=\; \sum_{i=1}^{m} {\omega_i}^2\,, \tag{13} $$

where m is the number of the eigenvalues kept. It is obvious that $Z \geq \tilde{Z}$, and the difference $Z - \tilde{Z}$ is fairly small when m is sufficiently large. We can also express $\tilde{Z}$ as

$$ \tilde{Z} = \mathrm{Tr}\,(P_L\,\rho_L) = \mathrm{Tr}\,\tilde{\rho}_L \tag{14} $$

where P_L is a projection operator

$$ P_L(\boldsymbol{s}'_L|\boldsymbol{s}_L) = \sum_{\xi=1}^{m} A(\boldsymbol{s}'_L|\xi)A(\boldsymbol{s}_L|\xi)\,, \tag{15} $$

and therefore $\tilde{\rho}_L$ is an m-dimensional diagonal matrix

$$ \tilde{\rho}_L(\xi'|\xi) = \sum_{\boldsymbol{s}'_L \boldsymbol{s}_L} A(\boldsymbol{s}'_L|\xi')\rho_L(\boldsymbol{s}'_L|\boldsymbol{s}_L)A(\boldsymbol{s}_L|\xi) \;=\; \delta_{\xi'\,\xi}\,\omega_\xi^2 \tag{16} $$

where $\xi', \xi \leq m$. (If $m = 2^M$, P_L coincides with I_L in Eq.10.) From Eqs.14-16, the transformation $\rho_L \to \tilde{\rho}_L$ by $A(\boldsymbol{s}_L|\xi)$ in Eq.16 can be regarded as the RG transformation from the row spin $\boldsymbol{s}_L$ to an m-state block spin ξ. In the same manner $B(\boldsymbol{s}_R|\zeta)$ is related to the RG transformation $\boldsymbol{s}_R \to \zeta$, that performs the mapping $\rho_R \to \tilde{\rho}_R$. In the following, we put '~' on top of the renormalized matrices.

It should be noted that the RG transformation $\rho_L \to \tilde{\rho}_L$ is performed so that it maximizes the approximate partition function $\tilde{Z}$ within the restricted freedom m. On the other hand, the RG transformation in quantum DMRG minimizes the ground state energy; this is consistent from the thermodynamic relation $F = -k_{\rm B}T \log Z = U - TS$ in the limit $T \to 0$.

4 Infinite System Algorithm

In quantum DMRG, the infinite system algorithm consists of the iterative use of the system expansion and the RG transformation for the Hamiltonian. It is easy to introduce the RG process to 2D classical system, using the quantum-classical correspondence $T^{(N)} = \exp(-\Delta H^{(N)})$; as far as the formulation is concerned, the classical DMRG can be obtained just by replacing the Hamiltonian $H^{(N)}$ in quantum DMRG to the transfer matrix $T^{(N)}$. As we show in this section, the infinite system algorithm construct renormalized transfer matrices $\tilde{T}^{(6)}, \tilde{T}^{(8)}, \ldots, \tilde{T}^{(N)}$ successively up to arbitrary N.

The infinite system algorithm starts from the 4-site system, whose transfer matrix is given by

$$T^{(4)}(s_1' s_2' s_3' s_4' | s_1 s_2 s_3 s_4) = T_L(s_1' s_2' | s_1 s_2) W(s_2' s_3' | s_2 s_3) T_R(s_3' s_4' | s_3 s_4)\,. \quad (17)$$

Diagonalizing $T^{(4)}$, we obtain the largest eigenvalue and the corresponding eigenvector $v^{(4)}(s_1 s_2 s_3 s_4)$, that satisfies $T^{(4)} v^{(4)} = \lambda\, v^{(4)}$. We then obtain $\rho_L(s_1' s_2' | s_1 s_2)$ and $\rho_R(s_3' s_4' | s_3 s_4)$ using Eq.8, and get the RG transformation matrices $A(s_1 s_2 | \xi)$ and $B(s_3 s_4 | \zeta)$ from the diagonalization of ρ_L and ρ_R. (Eq.11)

The next step is the system extension $N = 4 \to 6$ and the RG transformation via the substitution

$$\sum_{s_1' s_2' s_1 s_2} A(s_1' s_2' | \xi) T_L(s_1' s_2' | s_1 s_2) W(s_2' s_3' | s_2 s_3) A(s_1 s_2 | \xi) \to \tilde{T}_L(\xi' s_3' | \xi s_3)$$

$$\sum_{s_5' s_6' s_5 s_6} B(s_5' s_6' | \zeta) W(s_4' s_5' | s_4 s_5) T_R(s_5' s_6' | s_5 s_6) B(s_5 s_6 | \zeta) \to \tilde{T}_R(s_4' \zeta' | s_4 \zeta)\,, \quad (18)$$

where $\tilde{T}_L$ and $\tilde{T}_R$ are the renormalized half-row transfer matrices. (We have changed the spin indices of T_R according to the extension $N = 4 \to 6$.) The greek indices ξ and ζ represent the block spin variables, that are (at most) m state. Joining $\tilde{T}_L$ and $\tilde{T}_R$, we can construct the *extended* renormalized transfer matrix for $N = 6$

$$\tilde{T}^{(6)}(\xi' s_3' s_4' \zeta' | \xi s_3 s_4 \zeta) = \tilde{T}_L(\xi' s_3' | \xi s_3) W(s_3' s_4' | s_3 s_4) \tilde{T}_R(s_4' \zeta' | s_4 \zeta)\,. \quad (19)$$

At this stage, ξ and ζ represent the 2-spin blocks.

It is obvious that we can obtain $\tilde{T}^{(8)}$ in the same manner, i.e., diagonalizing $\tilde{T}^{(6)}$ in Eq.19 to obtain the largest eigenvalue and the corresponding

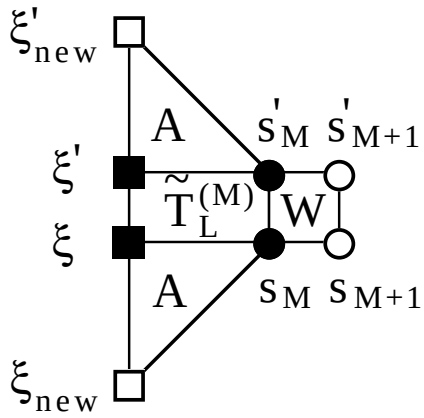

Fig. 4. Extension and the RG transformation for the half-row transfer matrix in Eqs.18-21, that is nessecary for the mapping $\tilde{T}^{(N)} \to \tilde{T}^{(N+2)}$.

eigenvector $\tilde{v}^{(6)}(\xi s_3 s_4 \zeta)$, and create $\tilde{\rho}_L(\xi' s'_3|\xi s_3)$ and to $\tilde{\rho}_R(s'_4\zeta'|s_4\zeta)$, using an extension of Eq.8. We obtain the RG transformations $A(\xi s_3|\xi_{\rm new})$ and $B(s_4\zeta|\zeta_{\rm new})$ by diagonalizing $\tilde{\rho}_L$ and $\tilde{\rho}_R$, (an extension of Eq.11) respectively, where $\xi_{\rm new}$ and $\zeta_{\rm new}$ are m-state variables that represent the 3-spin block. The $\tilde{T}^{(8)}$ is then constructed as

$$\begin{aligned}\tilde{T}^{(8)}&(\xi'_{\rm new}s'_4s'_5\zeta'_{\rm new}|\xi_{\rm new}s_4s_5\zeta_{\rm new})\\ &= \tilde{T}_L(\xi'_{\rm new}s'_4|\xi_{\rm new}s_4)W(s'_4s'_5|s_4s_5)\tilde{T}_R(s'_5\zeta'_{\rm new}|s_5\zeta_{\rm new})\,,\end{aligned} \tag{20}$$

where $\tilde{T}_L(\xi'_{\rm new}s'_4|\xi_{\rm new}s_4)$ and $\tilde{T}_R(s'_5\zeta'_{\rm new}|s_5\zeta_{\rm new})$ are created as

$$\begin{aligned}&\sum_{\xi' s'_3 \xi s_3} A(\xi' s'_3|\xi'_{\rm new})\tilde{T}_L(\xi' s'_3|\xi s_3)W(s'_3s'_4|s_3s_4)A(\xi s_3|\xi_{\rm new}) \to \tilde{T}_L(\xi'_{\rm new}s'_4|\xi_{\rm new}s_4)\\ &\sum_{s'_6\zeta' s_6\zeta} B(s'_6\zeta'|\zeta'_{\rm new})W(s'_5s'_6|s_5s_6)\tilde{T}_R(s'_6\zeta'|s_6\zeta)B(s_6\zeta|\zeta_{\rm new}) \to \tilde{T}_R(s'_5\zeta'_{\rm new}|s_5\zeta_{\rm new})\,.\end{aligned} \tag{21}$$

In this way, we further obtain $\tilde{T}^{(10)}$, $\tilde{T}^{(12)}$, $\tilde{T}^{(14)}$, ..., etc., up to arbitrary system size. This is the outline of the infinite system algorithm.

Numerical diagonalization for $\tilde{T}^{(N)}$ is normally performed via the Lanczos method, [26] that requires multiplication of $\tilde{T}^{(N)}$ to a $4m^2$-dimensional vector $\boldsymbol{x}$. Since $\tilde{T}^{(N)}$ is represented as a product of $\tilde{T}_L$, W, and $\tilde{T}_R$, the numerical multiplication $\boldsymbol{x}''' = \tilde{T}^{(N)}\boldsymbol{x}$ can be done very rapidly via the following 3 steps (Chap. 2(I))

$$x'(\xi' s'_M s_M s_{M+1}\zeta) = \sum_{\xi} \tilde{T}_L(\xi' s'_M|\xi s_M)x(\xi s_M s_{M+1}\zeta)\,, \tag{22}$$

$$x''(\xi' s'_M s'_{M+1} s_{M+1}\zeta) = \sum_{s_M} W(s'_M s'_{M+1}|s_M s_{M+1}) x'(\xi' s'_M s_M s_{M+1}\zeta)\,,$$

$$x'''(\xi' s'_M s'_{M+1}\zeta') = \sum_{s_{M+1}\,\zeta} \tilde{T}_R(s'_{M+1}\zeta'|s_{M+1}\zeta) x''(\xi' s'_M s'_{M+1} s_{M+1}\zeta)\,.$$

We don't have to explicitly prepare the $4m^2$-dimensional transfer matrix $\tilde{T}^{(N)}$, that contains $16m^4$ numbers of matrix elements. The Lanczos diagonalization can be further accelerated by an appropriate choice of the initial vector. [45–47]

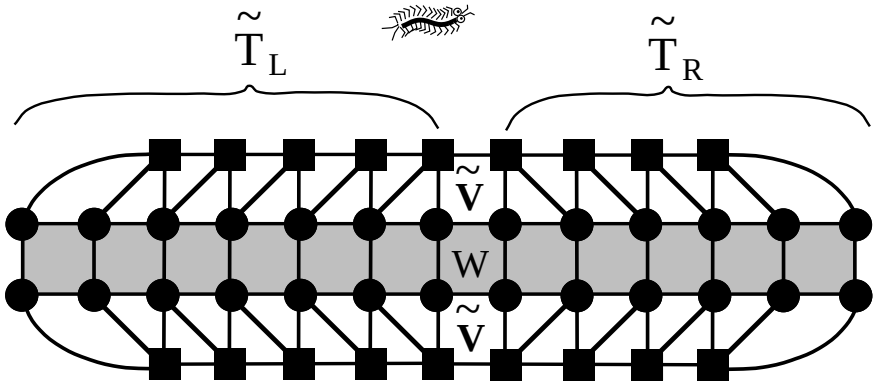

Fig. 5. Graphical representation of the variational eigenvalue of the transfer matrix $T^{(N)}$. (Eq.23) The shaded region represents $T^{(N)}$. The upper and lower parts correspond to the variational state $v^{(N)}$ in Eq.24.

5 Variational State in DMRG

At this point, it is possible to understand the variational nature of the classical (and also quantum) DMRG. Suppose that we have $\tilde{T}^{(N)}$ and the corresponding eigenvector $\tilde{v}^{(N)}(\xi s_M s_{M+1}\zeta)$ from the infinite system algorithm, where $\langle\tilde{v}^{(N)}|\tilde{v}^{(N)}\rangle = 1$ is satisfied. Figure 5 shows the graphical representation of $\tilde{\lambda} = \langle\tilde{v}^{(N)}|\tilde{T}^{(N)}|\tilde{v}^{(N)}\rangle$. The shaded regions represent $T^{(N)}(\boldsymbol{s'}|\boldsymbol{s})$. The left and the right halves of the figure correspond to $\tilde{T}_L(\xi' s'_M|\xi s_M)$ and $\tilde{T}_R(s'_{M+1}\zeta'|s_{M+1}\zeta)$, respectively. If we remind that $\tilde{T}_L$ and $\tilde{T}_R$ are created through the iterative use of Eq.21, it is possible to understand the relation

$$\langle\tilde{v}^{(N)}|\tilde{T}^{(N)}|\tilde{v}^{(N)}\rangle \;=\; \langle v^{(N)}|T^{(N)}|v^{(N)}\rangle\,, \tag{23}$$

where $v^{(N)}(s_{1\cdots}s_N)$ is the variational state for $T^{(N)}$ defined as

$$\sum_{\{\xi\}\{\zeta\}} \prod_{i=2}^{M-1} A(\xi_{i-1}s_i|\xi_i)\ \tilde{v}^{(N)}(\xi_{M-1}s_M s_{M+1}\zeta_{M+2}) \prod_{j=M+2}^{N-1} B(s_j\zeta_{j+1}|\zeta_j)\,, \quad (24)$$

where $\xi_1 \equiv s_1$ and $\zeta_N \equiv s_N$. We have put the indices to ξ and ζ in order to distinguish the block spin variables. The matrices $A(\xi_{i-1}s_i|\xi_i)$ and $B(s_j\zeta_{j+1}|\zeta_j)$ are dependent to their position i and j, respectively. Note that $v^{(N)}(s_{1\cdots}s_N)$ is normalized because of the assumed normalization $\langle\tilde{v}^{(N)}|\tilde{v}^{(N)}\rangle = 1$ and the orthogonal relations

$$\begin{aligned}
&\sum_{\xi_{i-1}s_i} A(\xi_{i-1}s_i|\xi_i)\,A(\xi_{i-1}s_i|\xi_i') \;=\; \delta_{\xi_i\,\xi_i'} \\
&\sum_{s_j\zeta_{j+1}}^{m} B(s_j\zeta_{j+1}|\zeta_j)B(s_j\zeta_{j+1}|\zeta_j') \;=\; \delta_{\zeta_j\,\zeta_j'}\,. \qquad (25)
\end{aligned}$$

Thus, the largest eigenvalue $\tilde{\lambda}$ of $\tilde{T}^{(N)}$ is the variational upper bound for the largest eigenvalue λ of $T^{(N)}$

$$\lambda \geq \tilde{\lambda} \;=\; \frac{\langle\tilde{v}^{(N)}|\tilde{T}^{(N)}|\tilde{v}^{(N)}\rangle}{\langle\tilde{v}^{(N)}|\tilde{v}^{(N)}\rangle} \;=\; \langle v^{(N)}|T^{(N)}|v^{(N)}\rangle\,, \quad (26)$$

and the difference $\epsilon = \lambda - \tilde{\lambda}$ is a decreasing function of m.

It is possible to further decompose $\tilde{v}^{(N)}(\xi_{M-1}s_M s_{M+1}\zeta_{M+2})$ into the matrix product, [27] and to write down the variational state in the form

$$\begin{aligned}
&v^{(N)}(s_{1\cdots}s_N) \\
&\qquad = \sum_{\{\xi\}\{\zeta\}} \prod_{i=2}^{M} A(\xi_{i-1}s_i|\xi_i)\ \Omega(\xi_M|\zeta_{M+1}) \prod_{j=M+1}^{N-1} B(s_j\zeta_{j+1}|\zeta_j)\,, \quad (27)
\end{aligned}$$

where $\Omega(\xi_M|\zeta_{M+1})$ is a $2m$-dimensional diagonal matrix

$$\Omega(\xi_M|\zeta_{M+1}) \;=\; \delta_{\xi_M\zeta_{M+1}}\,\frac{\omega_{\xi_M}}{\sqrt{\tilde{Z}}}\,. \quad (28)$$

We have imposed the normalization $\Omega^2 = 1$. (Strictly speaking, Ω need not to be diagonal, but $\Omega\Omega^T$ should be.) In the thermodynamic limit $N \to \infty$, the matrices $A(\xi_{i-1}s_i|\xi_i)$ and $B(s_j\zeta_{j+1}|\zeta_j)$ lose the position dependence, and the the variational state in Eq.27 coincides with Ostlund's matrix product state. (See Chap. 3(I))

As a result of infinite system algorithm, we obtain the variational free energy per site

$$\tilde{f} \;=\; -\frac{1}{N}k_{\rm B}T\,\log\tilde{\lambda} \quad (29)$$

and other thermodynamic quantities via the numerical derivative of $\tilde{f}$. Since we explicitly have the variational state $v^{(N)}(s_{1\cdots}s_N)$, (Eqs.24 and 27) we can calculate arbitrary spin correlation functions, such as $\langle s_i \rangle = \langle v^{(N)}|\hat{s}_i|v^{(N)}\rangle$ and $\langle s_i s_j \rangle = \langle v^{(N)}|\hat{s}_i\hat{s}_j|v^{(N)}\rangle$, etc. Generally speaking, the numerical precision of $\langle s_i s_j \rangle$ decreases as $|i-j|$ increases.

When we calculate spin correlation functions, we have to check that the energy scale ϵ_m introduced by the freedom restriction is sufficiently small compared with the excitation gap ϵ_g (of $H^{(N)} \equiv -\log \tilde{T}^{(N)}/\Delta$). If not, we have to increase m to keep the numerical precision. If the system is just at the critical temperature $T = T_{\rm c}$, the gap ϵ_g is of the order of $1/N$. For this reason, it is not realistic to apply the infinite system algorithm to a classical system just at $T_{\rm c}$, and directly analyze the thermodynamic limit $N \to \infty$. It would be better to use the finite system algorithm, that further improves the variational state obtained by the infinite system algorithm. (See §7.)

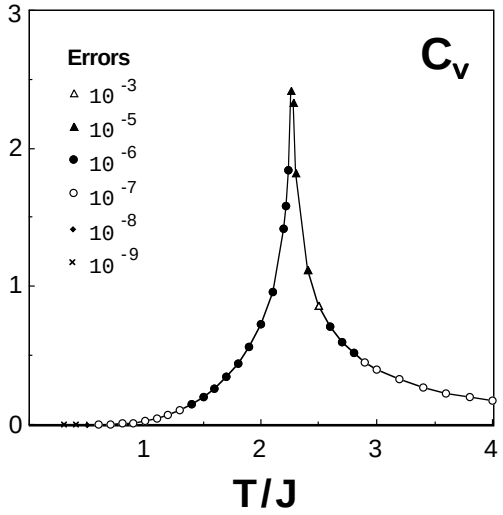

Fig. 6. Calculated specific heat of the Ising model. [5]

Let us see how precise the infinite system algorithm is. Figure 6 shows the specific heat $\mathrm{C_v}(T)$ of the square lattice Ising model, which is obtained by taking the temperature derivative of the nearest neighbor correlation function $E(T) = \langle s_M s_{M+1} \rangle$. We calculate $E(T)$ for the system up to $N = 2M = 2048$, which is sufficiently larger than the correlation length for each plotted temperature, except at $T = T_{\rm c}$. The m dependence for $E(T)$ is negligible when we keep $m = 60$ states. Since we know the exact solution for this model, [28] we can directly observe the numerical error in $\mathrm{C_v}(T)$; in Fig.6,

the order of error is indicated by several marks. The numerical error is non-negligible near the critical temperature $T_{\rm c}$, partly because $E(T)$ is singular at $T_{\rm c}$, and because the numerical derivative

$$\frac{E(T+\Delta T/2)-E(T-\Delta T/2)}{\Delta T} \tag{30}$$

is sensitive to ΔT; typically, we have chosen $\Delta T = 10^{-4}$. The other source of numerical error is that the increase of the cut-off energy scale ϵ_m near $T_{\rm c}$, that spoils the numerical precision of block spin transformation.

6 History of the Matrix Product State

Variational states written in the form of matrix product, such as $v^{(N)}$ in Eq.24, have been used for long time. In this section we review the brief history of the matrix product state. In 1941 Klamers and Wannier (K-W) [29,30] investigated the square lattice Ising model, assuming that the variatonal state can be written as

$$v(\dots,s_{i-1},s_i,s_{i+1},s_{i+2},\dots) = \dots F(s_{i-1}|s_i)F(s_i|s_{i+1})F(s_{i+1}|s_{i+2})\dots, \tag{31}$$

where $F(s'|s)$ is a 2-dimensional symmetric matrix. The calculated transition temperature $T_{\rm c}$ and the specific heat from this variational state are more accurate than those obtained by the molecular-field and the Bethe approximations. [31] It should be noted that the Gutzwiller approximation [32] for the Hubbard Model [33,34] is quite similar to the K-W approximation.

Around 1960-70 Baxter improved the K-W approximation by introducing additional freedom. [18,35] His variational state is written as

$$\begin{aligned} &v(\dots,s_{i-1},s_i,s_{i+1},s_{i+2},\dots) \\ &\quad = \sum_{\dots,a,b,c,d,\dots} \dots F_{ab}(s_{i-1}|s_i)F_{bc}(s_i|s_{i+1})F_{cd}(s_{i+1}|s_{i+2})\dots, \end{aligned} \tag{32}$$

where $\dots a$, b, c, $d\dots$, denote the additional m-state variables. Since $F_{ab}(s'|s)$ contains $4m^2$ adjustable parameters, the way of finding out the best $F_{ab}(s'|s)$ is non trivial. He performed the optimization using a self-consistent equation about the corner transfer matrix. (CTM) [18]

Applications of the matrix product formulation to quantum systems began with the investigations of Haldane's conjecture. In 1985 Nightingale and Blöte [36] used the K-W matrix product (Eq.31) as the initial vector of their projector Monte Carlo simulation. It is interesting that they commented about Baxter's method as "... *This method was formulated by Baxter for classical models in statistical mechanics. The generalization to quantum mechanical system is straightforward.*" (The RVA formulation by Sierra and Martìn-Delgado [37] can be seen as a realization of this conjecture; see

Chap. 4(I).) In 1987 Affleck, Lieb, Kennedy, and Tasaki [38] showed that the ground-state of a special $S = 1$ spin chain can be exactly expressed as

$$\sum_{\ldots,a,b,c,d,e,\ldots} \ldots M_{ab}(s_{i-1})M_{bc}(s_i)M_{cd}(s_{i+1})M_{de}(s_{i+2})\ldots , \tag{33}$$

where $\ldots, a, b, c, d, e, \ldots$ are 2-state variables. They also showed that ground state of this kind exists also for a two-dimensional $S = 3/2$ quantum spin system. Fannes *et al* generalized the above wave function (Eq.33) by assigning m-degree of freedom to $\ldots, a, b, c, d, e, \ldots$. Their variational state is known as 'finitely correlated state', since the correlation length is always finite. [39,40] Although Eq.33 does not look like Eq.32, they are essentially the same; they are related via a duality transformation. Such a product state has been considered independently in the field of the exclusion process. [41–44]

The variational states in Eqs.31-33 are uniform. The advantage of the variational state in DMRG (Eqs.24 and 27) is that it allows the position dependence for the matrices. Because of this, it is possible to treat finite size system in the framework of DMRG.

7 Finite System Algorithm

The variational state $v^{(N)}(s_{1\ldots}s_N)$ (Eq.24) obtained by the infinite system algorithm is a good approximation for the eigenvector of $T^{(N)}$, however, it is not the best one. The finite system algorithm improves the state, so that $\langle v^{(N)}|T^{(N)}|v^{(N)}\rangle$ is maximized under the constraint $\langle v^{(N)}|v^{(N)}\rangle = 1$, keeping at most m-state for each block spin variable.

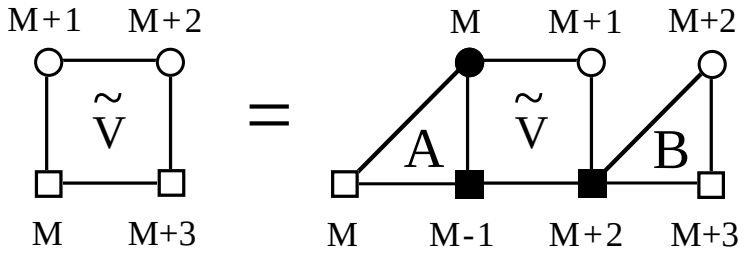

Fig. 7. Position shift of the renormalized state vector $\tilde{v}^{(N)}$ by way of Eqs. 35-36.

The algorithm gradually improves the whole part of the variational state

$$\sum_{\{\xi\}\{\zeta\}} \prod_{i=2}^{M-1} A(\xi_{i-1}s_i|\xi_i)\ \tilde{v}^{(N)}(\xi_{M-1}s_M s_{M+1}\zeta_{M+2}) \prod_{j=M+2}^{N-1} B(s_j\zeta_{j+1}|\zeta_j)\,. \tag{34}$$

directly improving the renormalized state $\tilde{v}^{(N)}$, and indirectly improving other parts by shifting the position of $\tilde{v}^{(N)}$. Assuming that we have already

obtained all of the matrices shown in Eq.34, we explain the following numerical procedures of the finite system algorithm of the classical DMRG; the main point is the position shift for $\tilde{v}^{(N)}$. [45,46] Let us create the DSM

$$\tilde{\rho}_L(\xi'_{M-1}s'_M|\xi_{M-1}s_M) = \sum_{s_{M+1}\zeta_{M+2}} \tilde{v}^{(N)}(\xi'_{M-1}s'_M s_{M+1}\zeta_{M+2})\,\tilde{v}^{(N)}(\xi_{M-1}s_M s_{M+1}\zeta_{M+2})\,, \quad (35)$$

and obtain $A(\xi_{M-1}s_M|\xi_M)$ by diagonalizing it. Then, by shifting the position of $\tilde{v}^{(N)}$ as shown in Fig.7

$$\tilde{v}^{(N)}(\xi_M s_{M+1}s_{M+2}\zeta_{M+3}) = \quad (36)$$
$$\sum_{s'_M\xi'_{M-1}\zeta'_{M+2}} \tilde{A}(\xi'_{M-1}s'_M|\xi_M)\tilde{v}^{(N)}(\xi'_{M-1}s'_M s_{M+1}\zeta'_{M+2})\tilde{B}(s_{M+2}\zeta_{M+3}|\zeta'_{M+2})\,,$$

we can construct the new variational state

$$v^{(N)}_{\rm new}(s_{1\cdots}s_N) = \quad (37)$$
$$\sum_{\{\xi\}\{\zeta\}} \prod_{i=2}^{M} A(\xi_{i-1}s_i|\xi_i)\ \tilde{v}^{(N)}(\xi_M s_{M+1}s_{M+2}\zeta_{M+3}) \prod_{j=M+3}^{N-1} B(s_j\zeta_{j+1}|\zeta_j)\,.$$

Compare Eq.37 with 34, the position of $\tilde{v}^{(N)}$ is shifted by one.

The finite system algorithm maximizes $\langle v^{(N)}_{\rm new}|T^{(N)}|v^{(N)}_{\rm new}\rangle$ via the tuning of $\tilde{v}^{(N)}(\xi_M s_{M+1}s_{M+2}\zeta_{M+3})$, under the constraint $\langle v^{(N)}_{\rm new}|v^{(N)}_{\rm new}\rangle = 1$. This maximization is equivalent to the diagonalization of the (shifted) renormalized transfer matrix

$$\tilde{T}^{(N)}(\xi'_M s'_{M+1}s'_{M+2}\zeta'_{M+3}|\xi_M s_{M+1}s_{M+2}\zeta_{M+3}) = \tilde{T}_L(\xi'_M s'_{M+1}|\xi_M s_{M+1})W(s'_{M+1}s'_{M+2}|s_{M+1}s_{M+2})\,\tilde{T}_R(s'_{M+2}\zeta'_{M+3}|s_{M+2}\zeta_{M+3}) \quad (38)$$

to obtain its eigenvector $\tilde{v}^{(N)}(\xi_M s_{M+1}s_{M+2}\zeta_{M+3})$, where we already have $\tilde{T}_R(s'_{M+2}\zeta'_{M+3}|s_{M+2}\zeta_{M+3})$, and the half-row transfer matrix $\tilde{T}_L(\xi'_M s'_{M+1}|\xi_M s_{M+1})$ can be easily obtained as

$$\sum_{\xi'_{M-1}s'_M\xi_{M-1}s_M} A(\xi'_{M-1}s'_M|\xi'_M)\tilde{T}_L(\xi'_{M-1}s'_M|\xi_{M-1}s_M)\,W(s'_M s'_{M+1}|s_M s_{M+1})A(\xi_{M-1}s_M|\xi_M) \quad (39)$$

Thus, by choosing $\tilde{v}^{(N)}$ in Eq.36 as the initial vector of the Lanczos diagonalization for $\tilde{T}^{(N)}$ in Eq.38, [45] we can rapidly improve $\tilde{v}^{(N)}(\xi_M s_{M+1}s_{M+2}\zeta_{M+3})$.

In such a way the finite system algorithm shifts the position of $\tilde{v}^{(N)}$ to the arbitrary place, and improves the variational state place by place. [48] This is the outline of the finite size algorithm; the numerical procedures are

basically the same as those in quantum DMRG, explained in Chap. 2(I). It is interesting that such a local improvement (or update) is also used in the zero-temperature QMC simulation for fermionic system. [49]

The advantage of finite system algorithm, compared to the infinite one, is its high numerical precision in the calculated thermodynamic quantities and spin correlation functions. The precision is high enough to determine the critical exponent of a classical system, with the help of finite size scaling. [50,51] Examples are shown in Chaps. 3.2(II) and 3.3(II) by Carlon and Drzewinski. [6–8]

8 Corner Transfer Matrix Formulation

We have treated the 2D Ising model on a cylinder, and applied the RG transformation to the transfer matrix $T^{(N)}$. Remember that the block spin transformation is obtained from the diagonalization of DSM, which corresponds to a cut on the cylinder. (Fig.3) The pictorial image of the DSM suggests that we can define DSM for any system with arbitrary geometry, just by creating a cut on it. Baxter established such a construction of DSM more than 30 years ago. [18,35] He considered a square cluster, and expressed the DSM of the system as the 4-th power of so called the corner transfer matrix. (CTM)

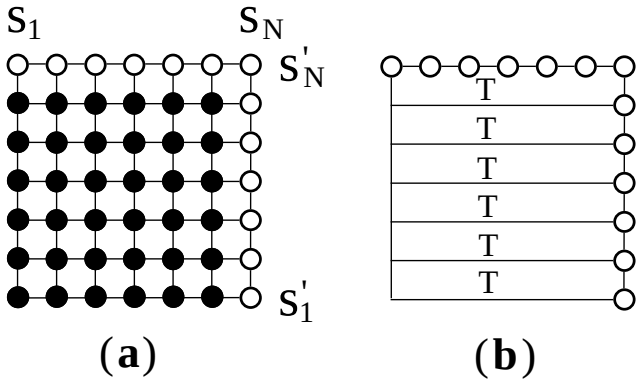

Fig. 8. Construction of the corner transfer matrix $C^{(N)}$. (Eq.40) (**a**) Configuration sum is taken over for the spins shown by black marks. (**b**) It is possible to regard $C^{(N)}$ as a stack of N pieces of $T^{(N)}$ with appropriate boundary conditions.

The CTM represent the Boltzmann weight of a square cluster. Figure 8 (**a**) shows the corner transfer matrix of the Ising model

$$C^{(N)}(\boldsymbol{s}'|\boldsymbol{s}) = \sum_{\{s\}} \prod_{\langle ijkl\rangle} W(s_i s_j | s_k s_l)\,, \tag{40}$$

where $\langle ijkl \rangle$ represents the neighboring spins around a plaquett W, and the sum is taken over for all the spins shown by black marks. By the definition, $C^{(N)}(\boldsymbol{s}'|\boldsymbol{s})$ is block diagonal, because s'_N in $\boldsymbol{s}' = s'_{1\ldots}s'_N$ and s_N in $\boldsymbol{s} = s_{1\ldots}s_N$ are the same; in other word, $C^{(N)}(\boldsymbol{s}'|\boldsymbol{s})$ for $s'_N \neq s_N$ is always zero. It is also possible to construct $C^{(N)}$ by stacking N numbers of transfer matrix $T^{(N)}$, and by imposing appropriate boundary conditions. (Fig. 8(**b**)) The area extension $C^{(N)}(\boldsymbol{s}'|\boldsymbol{s}) \to C^{(N+1)}(\boldsymbol{s}'_{\rm new}|\boldsymbol{s}_{\rm new}) = C^{(N+1)}(s'_{1\ldots}s'_{N+1}|s_{1\ldots}s_{N+1})$ is written as

$$C^{(N+1)}(\boldsymbol{s}'_{\rm new}|\boldsymbol{s}_{\rm new}) = \sum_{\boldsymbol{s}'''\boldsymbol{s}''} \delta_{s'_{N+1}s_{N+1}} W(s_N s_{N+1}|s''_N s'_N) \\ T^{(N)}(\boldsymbol{s}'|\boldsymbol{s}''')T^{(N)}(\boldsymbol{s}|\boldsymbol{s}'')C^{(N)}(\boldsymbol{s}'''|\boldsymbol{s}'')\,. \tag{41}$$

The position of the spin variables are shown in Fig.9.

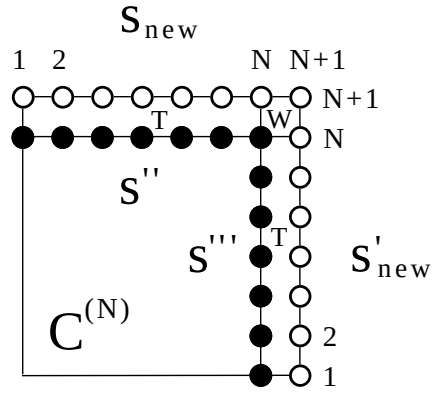

Fig. 9. Extension of the CTM: $C^{(N+1)}$ is obtained by joining two $T^{(N)}$ and a W on top of $C^{(N)}$. (Eq.41)

Baxter constructed the DSM as the 4-th power of the CTM

$$\rho_{\rm c}(\boldsymbol{s}''''|\boldsymbol{s}) = \sum_{\boldsymbol{s}'''\boldsymbol{s}''\boldsymbol{s}'} C^{(N)}(\boldsymbol{s}''''|\boldsymbol{s}''')C^{(N)}(\boldsymbol{s}'''|\boldsymbol{s}'')C^{(N)}(\boldsymbol{s}''|\boldsymbol{s}')C^{(N)}(\boldsymbol{s}'|\boldsymbol{s})\,. \tag{42}$$

This is not far from the conventional definition of DSM in DMRG (Eq.8), because $\rho_{\rm c}$ can be written as

$$\rho_{\rm c}(\boldsymbol{s}'_L|\boldsymbol{s}_L) = \sum_{\boldsymbol{s}_R} v(\boldsymbol{s}'_L|\boldsymbol{s}_R)v(\boldsymbol{s}_L|\boldsymbol{s}_R)\,, \tag{43}$$

where the vector $v(\boldsymbol{s}_L|\boldsymbol{s}_R)$ is given by

$$v(\boldsymbol{s}_L|\boldsymbol{s}_R) = \sum_{\boldsymbol{s}} C^{(N)}(\boldsymbol{s}_L|\boldsymbol{s})C^{(N)}(\boldsymbol{s}|\boldsymbol{s}_R)\,. \tag{44}$$

Note that $v(\boldsymbol{s}_L|\boldsymbol{s}_R)$ is block diagonal, as $C^{(N)}(\boldsymbol{s}'|\boldsymbol{s})$ is. Figure 10 shows the graphical representation of $\rho_{\rm c}$, that corresponds to a $2N-1$ by $2N-1$ square with a cut, where the cut extends from a side to the center. Thus $Z^{(2N-1)} = \mathrm{Tr}\,\rho_{\rm c}$ is the partition function of the $2N-1$ by $2N-1$ square system.

Using the CTM, Baxter calculated the variational free energy (per site) of 2D lattice models in the limit $N \to \infty$ by solving a self-consistent equation. Okunishi pointed out that Baxter's method is basically the same as the infinite system algorithm of the classical DMRG. [52] Compare to the classical DMRG, Baxter's method has an advantage that the numerical calculation is very fast, since it does not require diagonalizations of large scale matrices. Nishino and Okunishi introduced this advantage to DMRG, and formulated a numerical RG algorithm, which is called as 'corner-transfer-matrix renormalization group' (CTMRG). [53,54]

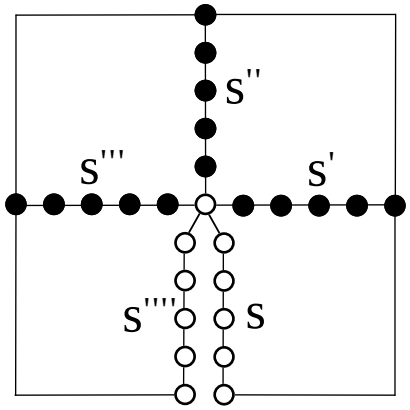

Fig. 10. Baxter's construction of the DSM as the 4-th power of CTM. (Eq.42)

The outline of the CTMRG is as follows. The diagonalization of the DSM

$$\rho_{\rm c}(\boldsymbol{s}'|\boldsymbol{s}) \;=\; \sum_{\xi} A(\boldsymbol{s}'|\xi)\,\alpha_\xi^4\,A(\boldsymbol{s}|\xi) \tag{45}$$

defines the RG transformation $\boldsymbol{s} \to \xi$ via the orthogonal matrix $A(\boldsymbol{s}|\xi)$. For example, $C^{(N)}$ can be renormalized as

$$\tilde{C}^{(N)}(\xi'|\xi) \;=\; \sum_{\boldsymbol{s}'\,\boldsymbol{s}} A(\boldsymbol{s}'|\xi')C^{(N)}(\boldsymbol{s}'|\boldsymbol{s})A(\boldsymbol{s}|\xi) \;=\; \delta_{\xi'\,\xi}\,\alpha_\xi\,, \tag{46}$$

where ξ' and ξ are m-state block spin variables. One thing we have to be careful is that $\rho_{\rm c}$ is block diagonal, as $C^{(N)}$ is, and therefore the block spin

ξ implicitly includes the spin variable s_N. The variational partition function of the $2N-1$ by $2N-1$ square is then expressed as

$$\tilde{Z}^{(2N-1)} = \mathrm{Tr}\,\tilde{\rho}_{\mathrm{c}} = \mathrm{Tr}\,\left(\tilde{C}_{\mathrm{c}}^{(N)}\right)^4 = \sum_{\xi=1}^{m} \alpha_\xi^4 \,. \tag{47}$$

As the infinite system algorithm, the CTMRG performs the successive mapping $\tilde{C}^{(N)} \to \tilde{C}^{(N+1)} \to \tilde{C}^{(N+2)}$ using the system size extension (Eq.41) and the RG transformation (Eq.46). As a result, we obtain $\tilde{Z}^{(2N-1)} \to \tilde{Z}^{(2N+1)} \to \tilde{Z}^{(2N+3)} \to \cdots$ up to arbitrary system size, starting from a small N (= 2 or 3).

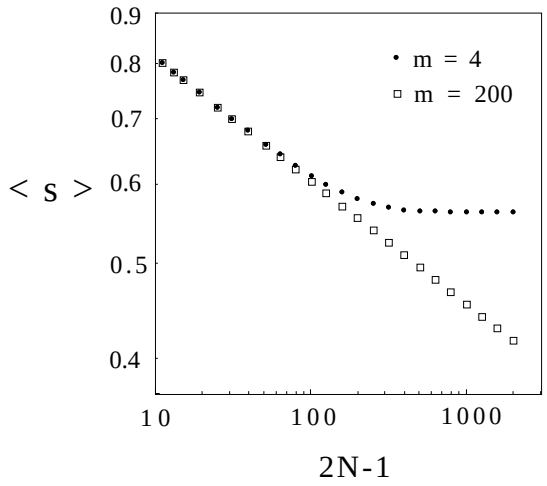

Fig. 11. Order parameter of the Ising model at the center of $2N-1$ by $2N-1$ square when $T = T_{\mathrm{c}}$.

Numerical data calculated by CTMRG is useful to the finite size scaling analyses of classical systems. Figure 11 shows the N-dependence of the local order parameter $\langle s \rangle$ of the Ising model at the center of $2N-1$ by $2N-1$ square, when $T = T_{\mathrm{c}}$. Fixed boundary condition (all spin up at the boundary) is chosen. We plot representative data for both $m = 4$ and $m = 200$ up to $2N-1 = 1999$. At the criticality, the local order parameter obeys the scaling formula

$$\langle s \rangle \propto (2N-1)^{-(d-2+\eta)/2} \,, \tag{48}$$

where d is the spatial dimension (= 2). In deed, the calculated parameter $\langle s \rangle$ is almost proportional to $(2N-1)^{-1/8}$. The least-square fitting to the data in the range $199 \le 2N-1 \le 19999$ gives $\eta = 0.2501$, which is quite close to the exact one $\eta = 1/4$. In the same manner, we can determine another

exponent ν from the nearest neighbor spin correlation $E_{2N-1} = \langle s's \rangle$ at the center of the $2N-1$ by $2N-1$ system, that obeys the scaling form

$$E_{2N-1} - E_\infty \propto (2N-1)^{1/\nu - d} . \tag{49}$$

From the calculated data for $199 \leq 2N-1 \leq 19999$, we obtain $\nu = 1.0006$. Again, the numerical result agrees with the exact exponent $\nu = 1$.

CTMRG is also useful to detect the latent heat L. As an example, let us calculate L of the $q = 5$ Potts model, [55] which shows the weak first order transition. (It was impossible to determine L by the Monte Carlo simulation, because L is quite small.) Figure 12 shows the calculated local energy at the center of $2N-1$ by $2N-1$ square system for both fixed (= ordered) and free (= disordered) boundary conditions, up to $2N-1 \leq 3999$ for $m = 40, 67$ and 200. Though there is non-negligible m-dependence, it is clear that the model does not show the second order transition. The double extrapolation with respect to N and m gives the latent heat $L = 0.027$ which agrees with the exact result $L \sim 0.0265$. [18,20] This is the first quantitative numerical estimate of L for the $q = 5$ potts model.

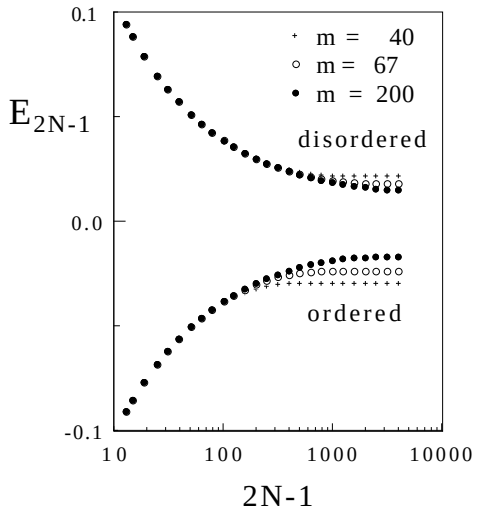

Fig. 12. Local energy E_{2N-1} of the $q = 5$ Potts model at the center of $2N-1$ by $2N-1$ square, calculated for both ordered and disordered phase, where energy zero is shifted to the average of disordered and ordered energies. [18,20]

Finally we comment that Baxter's construction of DSM can be generalized to any dimension. [56] For example, consider a cubic cluster of 3D Ising model, and divide it into 8 subcubes. (The original cube = stack of 8 subcubes.) As a direct extension of the CTM in 2D, we can imagine 'corner tensors' $C^{(N)}(a|b|c)$, that corresponds to the Boltzmann weight for a subcube; the tensor indices $a = (a_{ij})$, $b = (b_{ij})$, and $c = (c_{ij})$ represent 2D spin

arrays on the surfaces of the subcubes. Figure 13 shows the pictorial image of the DSM $\rho_{\rm cube}(a|b)$, which is constructed as a contruction between 8 corner tensors. In 3D, the DSM corresponds to a cut on the cube. We obtain the RG transformation from the surfaces a, b, and c to m-state block spins by diagonalizing $\rho_{\rm cube}(a|b)$. The size extension of the corner cube can be performed via a 3D generalization of Fig.9. Thus, as far as the formulation is concerned, we can extend CTMRG to 3D systems.

More Generally, by breaking up n-dimensional *hypercube* into 2^n-numbers of *hyper-corner-cubes*, we can define a DSM for $n-1$-dimensional surface of the hyper-corner cube. Once we obtain the DSM, we can define the block-spin transformation, and can apply RG transformations to the hypercubic system. Since the renormalized *hyper-corner tensor* has m^n numbers of elements, numerical calculations in higher dimension is much heavier than that in 2D.

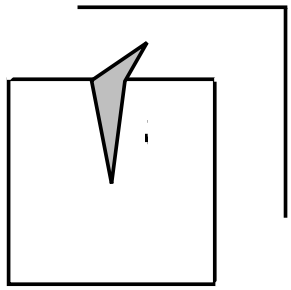

- It is not straightforward to treat random classical systems, because the transfer-matrix eigenvalue can be negative, and because the RG transformation depends on the position of block spins. [58]
- To treat a system with continuous site variable or a system defined in the continuous space (-time), we have to first discretize them; [59] we don't know the general principle for such a discretization, that is suitable for DMRG.

We hope that these problems will be solved near future.

The authors thank to the organizers of DMRG '98 workshop at Max-Planck-Institute für Physik komplexer System in Dresden. T. N. thank to I. Peschel, E. Carlon, G. Sierra, M. A. Martìn-Delgado, X. Wang and T. Xiang about the discussions for classical DMRG. Numerical calculations were done using NEC SX-4 in the computer center of Osaka University. Y. H. is partly supported by the Sasakawa Scientific Research Grant from The Japan Science Society. K. O. and T. H. partially supported by a Grant-in-Aid from the Ministry of Education, Science and Culture of Japan.

References

1. S. R. White: Phys. Rev. Lett. **69**, 2863(1992); Phys. Rev. **B 48**, 10345 (1993); Chap. 2(I).
2. H. F. Trotter: Proc. Am. Math. Soc. **10**, 545 (1959).
3. M. Suzuki: Prog. Theor. Phys. **56**, 1454 (1976).
4. R. P. Feynmann and A. R. Hibbs: Quantum Mechanics and Path Integrals (McGraw-Hill, 1965).
5. T. Nishino, J. Phys. Soc. Jpn. **64**, 3598 (1995).
6. Enrico Carlon and Andrzej Drzewiński: Phys. Rev. Lett. **79** (1997) 1591; Phys. Rev. **E57**, 2626 (1998); Chap. 3.2(II).
7. Enrico Carlon and Ferenc Igloi: Phys. Rev. **B 57**, 7877 (1998); Ferenc Igloi and Enrico Carlon: cond-mat/9805083.
8. Enrico Carlon, Andrzej Drzewiński and Jos Rogiers: cond-mat/cond-mat/9803193.
9. R. J. Bursill, T. Xiang, G. A. Gehring: J. Phys. Condensed Matter L583-L590 (1996).
10. X. Wang and T. Xiang, Phys. Rev. **B56** 5061 (1997); Chap. 6(I).
11. F. Naef, X. Wang, X. Zotos, and W. van der Linden; cond-mat/9812117.
12. N. Shibata, J. Phys. Soc. Jpn **66**, 2221 (1997); Chap. 4(II).
13. B. Ammon, M. Troyer, T.M. Rice, and N. Shibata; cond-mat/9812144.
14. Y. Honda and T. Horiguchi, cond-mat/9704002.
15. S. Östlund and S. Rommer: Phys. Rev. Lett **75**, 3537 (1995); S. Rommer and S. Östlund: Phys. Rev. **B55**, 2164 (1997); M. Andersson, M. Boman, and S. Östlund: cond-mat/9810093; Chap. 3(I)
16. It is possible to fix the boundary spins to consider more general boundary conditions.
17. There is a bibliography of Ising in cond-mat/9605174.

18. R. J. Baxter: Exactly Solved Models in Statistical Mechanics (Academic Press, London, 1982).
19. R. B. Potts: Proc. Camb. Phil. Soc.**48** 106.
20. F. Y. Wu: Rev. Mod. Phys. **54**, 235 (1982), and references there in.
21. Baxter used another definition of the density submatrix in his variational method, [18] where his density submatrix is block diagonal. (See Eqs.42-44.)
22. T. Nishino and K. Okunishi, in Strongly Correlated Magnetic and Superconducting Systems, Ed. G. Sierra and M. A. Martín-Delgado (Springer Berlin, 1997).
23. Eigenvalues of the DSM can be negative when the system contains randomness.
24. I. Peschel, M. Kaulke, and Ö. Legeza: cond-mat/9810174; Chap. 3.1(II)
25. Strictly speaking, the density matrix eigenvalues do not decay exponentially; See K. Okunishi, Y. Hieida, and Y. Akutsu: cond-mat/9810239.
26. C. Lanczos: J. Res. Nat. Bur. Std. **45**, 255 (1950).
27. The Numerical recipes Home Page (http://cfata2.harvard.edu/numerical-recipes/) is useful to know about numerical linear algebra. Also it is worth reading J. Wilkinson: The Algebraic Eigenvalue Problem (Oxford, London, 1965).
28. L. Onsager: Phys. Rev. **65**, 117 (1944).
29. H. A. Kramers and G. H. Wannier: Phys. Rev. **60**, 263 (1941).
30. R. Kikuchi: Phys. Rev. **81**, 988 (1951).
31. H. A. Bethe: Proc. Roy. Soc. **A150**, 552 (1935).
32. M. C. Gutzwiller: Phys. Rev. **137**, A1726 (1965).
33. J. Kanamori: J. Phys. Soc. Jpn. **30**, 275 (1963).
34. J. Hubbard: Proc. Roy. Soc. **A276**, 238 (1963); **A281**, 401 (1964).
35. R. J. Baxter: J. Math. Phys. **9**, 650 (1968); R. J. Baxter: J. Stat. Phys. **19**, 461 (1978).
36. N. P. Nightingale and H. W. Blöte: Phys. Rev. **B33**, 659 (1986).
37. G. Sierra and M. A. Martín-Delgado, Chap. 4(I).
38. I. Affleck, T. Kennedy, E. H. Lieb and H. Tasaki: Phys. Rev. Lett. **59**, 799 (1987).
39. M. Fannes, B. Nachtergale and R. F. Werner: Europhys. Lett. **10**, 633 (1989); M. Fannes, B. Nachtergale and R. F. Werner: Commun. Math. Phys. **144**, 443 (1992); M. Fannes, B. Nachtergale and R. F. Werner: Commun. Math. Phys. **174**, 477 (1995).
40. A. Klümper, A. Schadschneider and J. Zittarz: Z. Phys. **B87**, 281 (1992); H. Niggemann, A. Klümper and J. Zittartz: Z. Phys. **B104**, 103 (1997).
41. B. Derrida and M. R. Evans : J.Phys.A: Math. Gen. **26**, 1493 (1993).
42. N. Rajewsky, L. Santen, A. Schadschneider, M. Schreckenberg; cond-mat/9710316.
43. A. Honecker, I. Peschel: J. Stat. Phys. **88**, 319 (1997).
44. Y. Hieida; preprint.
45. S. R. White: Phys. Rev. Lett. **77**, 3633 (1996); Chap. 2(I)
46. T. Nishino and K. Okunishi: J. Phys. Soc. Jpn. **64**, 4084 (1995).
47. U. Schollvöck, cond-mat/9804231.
48. A modification of the whole part of the variational state is more time consuming. The situation is similar to the 'Order N' problem in the density functional formalism.
49. S. R. White, D. J. Scalapino, R. L. Sugar, E. Y. Loh, J. E. Gubernatis and R. T. Scalettar: Phys. Rev. **B40**, 506 (1989).

50. M. E. Fisher: in Proc. Int. School of Physics 'Enrico Fermi', edited by M.S. Green, (Academic Press, New York, 1971), Vol. **51**, p. 1.
51. M. N. Barber: in Phase Transitions and Critical Phenomena, edited by C. Domb and J. L. Lebowitz, (Academic Press, New York, 1983), Vol. **8**, p. 146. and references therein.
52. K. Okunishi: Thesis, Osaka University 1996 (in Japanese); Thesis, Osaka University 1999 (in English).
53. T. Nishino and K. Okunishi: J. Phys. Soc. Jpn. **65**, 891 (1996); T. Nishino and K. Okunishi: J. Phys. Soc. Jpn. **66**, 3040 (1997).
54. T. Nishino, K. Okunishi, and M. Kikuchi: Physics Letters **A213**, 69 (1996).
55. T. Nishino and K. Okunishi: J. Phys. Soc. Jpn. **67**, 1492 (1998).
56. T. Nishino and K. Okunishi: J. Phys. Soc. Jpn. **67**, 3066 (1998).
57. Numerical precision in DMRG for a system with periodic boundary condition is lower than that for the system with open boundary condition. The reason can be understood by looking at the variational state written in matrix product.
58. Position dependence *in quantum Hamiltonian* can be treated by quantum DMRG; K. Hida: J. Phys. Soc. Jpn. **65**, 895 (1996).
59. S. G. Chung: J. Phys. Cond. Matt. **9** L619 (1997); *Current Topics in Physics* ed. Y. M. Cho, J. B. Hong, and C. N. Yang, vol. **1** (World Scientific, Hongkong, 1998) p.295.